

Control-Oriented Modeling Requirements of a Direct-Drive Machine Tool Axis

Michael A. Stephens

ANCA Motion,
1 Bessemer Road, Bayswater North,
Victoria 3153, Australia

Chris Manzie

Malcolm C. Good

Department of Mechanical Engineering,
The University of Melbourne,
Victoria 3010, Australia

The high performance demands on commercial computer numerical control (CNC) machine tools have led to the widespread adoption of direct-drive servo axes. In industrial machines, where the workpiece is manipulated by the axis, the plant dynamics seen by the control system may vary widely between different workpieces. These changing plant dynamics have been observed to lead to limit-cycle behavior for a given controller. In such a situation, conventional modeling approximations used by practitioners may fail to predict the onset of instability for these axes. This work demonstrates the failure of conventional modeling approximations to predict the observed instability in an industrial CNC servo axis and investigates the model fidelity required to replicate the observations. This represents an important consideration when designing model-based controllers for direct-drive axes in CNC machines. [DOI: 10.1115/1.4006216]

1 Introduction

Globally, the accuracy and cycle time demands on high precision CNC machine tools are growing at a significant rate as manufacturers seek to gain a competitive advantage. As these automation systems become increasingly dependent on simulation and model-based control approaches, there is significant motivation for the development of low-order models that capture the key characteristics of machine tool servo drive axes; however, using component specifications to develop the models inevitably leads to high-order models [1]. Instead, the conventional approach in modeling the drive and workpiece is to postulate a model structure and perform system identification [2,3], to develop a low-order plant model that can be analyzed or used in controller design.

The control challenges and/or industrial approaches associated with nonrigid axes have been previously documented, for example in Refs. [4–8], and focus on methods for compensating for mechanical resonance in the plant models. The controller implementation in commercial machine tools is typically a statically tuned system that is required to handle all the variability the plant will encounter, because it is unproductive for the machine builder or operator to retune axes using conventional techniques on machines in use in remote locations throughout the world. The models used in designing position controllers for the axes typically make *explicit* assumptions of constant system dynamics and *implicitly* use principles of time scale separation [2,7].

Contributed by the Dynamic Systems Division of ASME for publication in the JOURNAL OF DYNAMIC SYSTEMS, MEASUREMENT, AND CONTROL. Manuscript received November 22, 2010; final manuscript received January 6, 2012; published online June 5, 2012. Assoc. Editor: Marcelo J. Dapino.

Over the last decade, there has been a trend in high performance machine tools to incorporate direct-drive servo axes. This configuration eliminates backlash, reduces friction, and improves acceleration. However, in contrast with geared systems, the direct-drive motor experiences the unattenuated effect of changes in load inertia and disturbances. Servo axes that are especially susceptible are those where large cutting forces are routinely experienced (such as on milling and grinding machines) or the range of workpieces used in the axis is subject to significant variation. One real world example highlighting the range of workpieces encountered by an industrial machine in the field is shown in Fig. 1. This illustrates that the explicit modeling assumption of constant plant dynamics cannot be maintained for direct-drive axes and consequently demonstrates the challenges facing a static controller implementation.

One phenomenon that has been anecdotally observed on industrial direct-drive axes operating under these conditions is the onset of limit-cycle behavior or hunting following a small perturbation when the axis is under position control. Such a situation occurs when the workpiece shown on the left-hand side of Fig. 1 is replaced with the one on the right-hand side without retuning the axis. Figure 2 depicts the onset of the limit-cycle behavior that is observed with the axis under closed-loop position control and a fixed position reference. Note that the axis begins to oscillate at approximately 410 Hz *in free air* before the machining operation even commences. If the machine is allowed to complete the machining operation in this state, then in the best case, the result is a workpiece with poor surface finish, and in the worst case, geometric accuracy outside acceptable tolerances, or even a broken tool or chipped grinding wheel.

Potential causes of this limit-cycle behavior might reasonably be suggested as issues related to nonlinear friction [9] or encoder quantization [10]. The former can be dismissed in this instance as the system starts from rest and there is no “stick-slip” dwell when the velocity passes through zero in Fig. 2; while, the latter is associated more with low-resolution sensors—the commercial system of Fig. 1 utilizes an encoder with an effective resolution of 1.5×10^{-5} deg.

In identifying the true cause of the observed instability in Fig. 2, there are several steps described in this paper. Initially, a procedure for identifying a suitable low-order plant model is proposed for a given workpiece, and standard analysis techniques are used to demonstrate that the observed closed-loop instability is *not* predicted when the workpiece is changed. The conventional modeling assumptions and their implication for stability are then assessed, and a model capable of predicting the onset of the limit-cycle behavior is derived. The result has clear implications for the requirements on model fidelity when using model-based design techniques for direct-drive axes.

2 Analysis Using Conventional Modeling Assumptions

The system considered in this paper is the workpiece-holding direct-drive rotary axis of the commercially available tool and cutter grinding machine shown in Fig. 1. The axis incorporates a permanent magnet synchronous motor (PMSM), where dq -vector control is used to orient the magnetic field so as to generate the required torque to position the axis. The key objective of this approach is to drive the d -axis current (i_d) to zero and control the q -axis current (i_q) to produce the required torque [11].

A block diagram of the closed-loop system to be analyzed is presented in Fig. 3, where θ_r is the motor position reference; ω_r is the motor velocity reference; i_r is the q -axis current reference; v_d and v_q are the d -axis and q -axis stator voltages; θ_m is the motor position, and ω_m is the motor velocity. Note also that the cascaded controller blocks have different sample periods, with fundamental sample period T . The ratio between the sample periods used by the current controller and the other nested loops is denoted by P . Sections 2.1–2.3 will develop a low-order plant and controller model using standard assumptions, and from these attempt to predict the observed instability in Fig. 2.

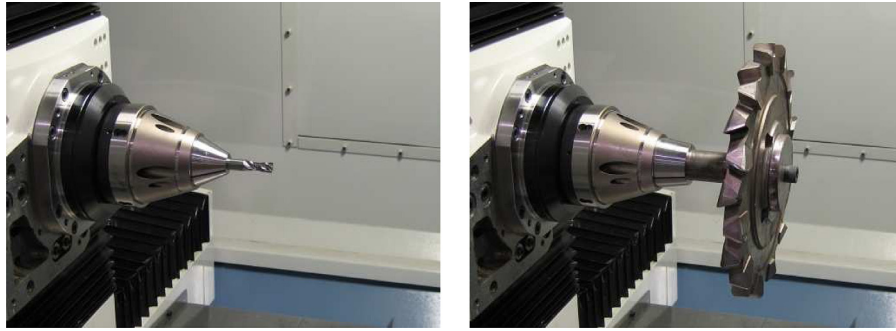


Fig. 1 Headstock servo axis of a tool and cutter grinding machine loaded with both small (left) and large (right) workpieces. The small workpiece is a 10 mm end mill, while the large workpiece is a 300 mm side-and-face cutter mounted to the headstock via a 32 mm arbor (shaft).

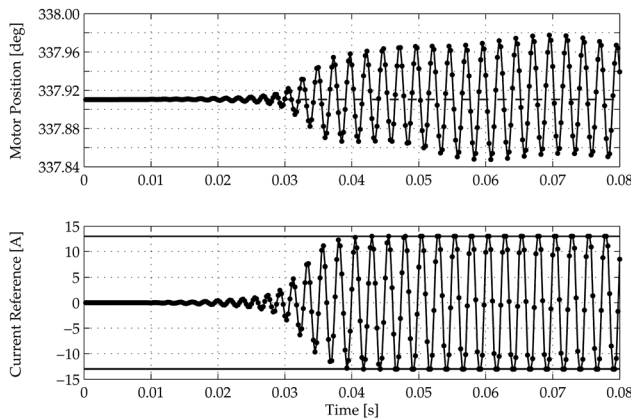


Fig. 2 Experimentally observed limit-cycle behavior during stationary operation of the axis loaded with the large workpiece. The position reference is the dashed line and the measured position is the solid line. The motor current saturation limits are also shown. The frequency of the observed oscillations is approximately 410 Hz.

2.1 Controller Model. The overall control algorithm is known and executes deterministically on a digital signal processor (DSP). In order to facilitate the analysis of this part of the system, computation delays and the dynamics of the fast sample-rate components (e.g., anti-aliasing filters, current reference filters, and the current controller) are typically either ignored [2,7] or simplified by a low-order continuous-time transfer function [5,12]. For the purposes of this section, the former option is chosen.

The position controller is a proportional controller, with gain K_{pos} . The velocity controller is proportional plus integral with gain K_{vel} and integral time constant T_i . Both of these controllers have a sample period of $PT = 250 \mu s$. For this axis, the default values for the controller parameters in Table 1 are chosen (by the commercial machine builder) to maximize the closed-loop bandwidth of each respective loop, while still maintaining a degree of gain margin to achieve reasonable robustness to unknown plant

Table 1 Default controller tuning parameters

Parameter	Value	Unit
K_{pos}	3.6111	rpm/deg
K_{vel}	0.4444	A/rpm
T_i	2000	μs
T	50	μs
P	5	—

dynamics. These controller gains ensure that high machining tolerances are maintained in the presence of disturbances. Further gain reduction may lead to stable responses when considering different plant dynamics, but come at the cost of unacceptable disturbance rejection performance.

2.2 Plant Model. The servo plant is composed of electrical and mechanical components. The electrical system consists of the high voltage power supply, the switching electronics, the current sensing, and the windings of the PMSM. The analog current signals are fed into low-pass anti-aliasing filters with an effective cutoff frequency of 6 kHz. The filtered signal is then sampled at 20 kHz. These filters are outside the digital system, and hence their dynamics are included in the electrical system. The electrical system is often the most complex part of the model, involving many nonlinear elements. However, it is typically assumed that the electrical and the mechanical dynamics are of sufficiently different time scales that the electrical system may be ignored.

The mechanical plant is in actuality continuously elastic, but is typically modeled as an interconnection of rigid bodies connected via spring-damper elements. To determine the appropriate model order, a commercial finite element analysis package was used to identify the vibrational modes up to the Nyquist frequency of the position and velocity controllers. From a modal analysis carried out on the axis with large workpiece (shown on the right-hand side of Fig. 1), two torsional modes were identified at frequencies less than the Nyquist frequency. Figure 4(a) shows the axial twist along the length of the axis/workpiece in the first torsional mode, Fig. 4(b) shows the second torsional mode, and Fig. 4(c) shows a

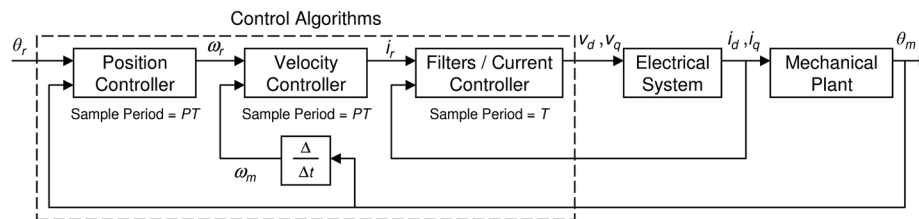


Fig. 3 Machine tool servo drive control loop structure

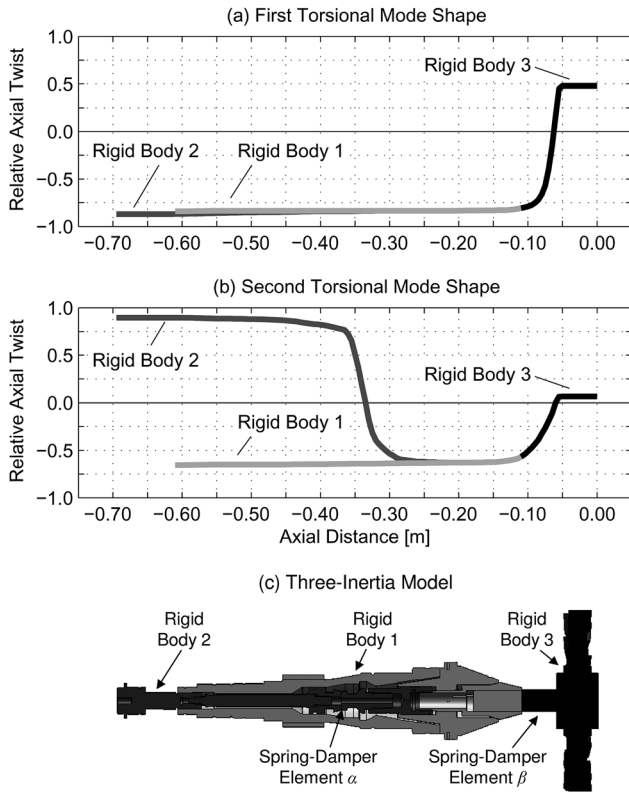


Fig. 4 Finite element modal analysis of the servo drive axis loaded with the large workpiece

cross-section view of the 3D computer-aided design (CAD) model that is shaded to correspond to the different sections of the mode shape graphs. From the graphs shown in Figs. 4(a) and 4(b), it is possible to identify three segments where the slope of the lines is essentially zero. These segments correspond to sections of the mechanical plant which, in this frequency range, can be well approximated as rigid bodies with angular positions θ_1 , θ_2 , and θ_3 , by

$$J_1 \ddot{\theta}_1 = K_t i_q - B_m^* \dot{\theta}_1 - [k_x(\theta_1 - \theta_2) + c_x(\dot{\theta}_1 - \dot{\theta}_2)] - [k_\beta(\theta_1 - \theta_3) + c_\beta(\dot{\theta}_1 - \dot{\theta}_3)] \quad (1a)$$

$$J_2 \ddot{\theta}_2 = [k_x(\theta_1 - \theta_2) + c_x(\dot{\theta}_1 - \dot{\theta}_2)] \quad (1b)$$

$$J_3 \ddot{\theta}_3 = [k_\beta(\theta_1 - \theta_3) + c_\beta(\dot{\theta}_1 - \dot{\theta}_3)] \quad (1c)$$

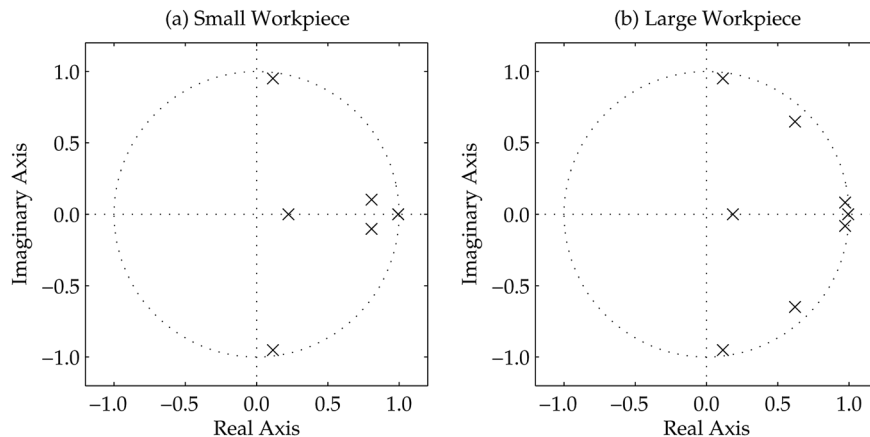


Fig. 5 Closed-loop poles of the motor position loop for the discrete model of the servo drive axis loaded with both small and large workpieces

Table 2 Experimentally identified model parameters

Parameter	Value	Unit
K_t	3.5801	N m/A
J_1	0.0127	Kg m ²
J_2	0.0002	Kg m ²
J_3 large workpiece	0.0500	Kg m ²
J_3 small workpiece	0	Kg m ²
B_m^*	0.0264	N m/(rad/s)
c_x	0.0658	N m/(rad/s)
c_β	0.6309	N m/(rad/s)
k_x	73,570	N m/rad
k_β	78,603	N m/rad

where J_1 and J_2 are the inertias of the two sections of the motor shaft, and J_3 is the inertia of the large workpiece head; k_x and k_β are the torsional stiffnesses, and c_x and c_β are the torsional damping coefficients of the two elastic coupling elements; K_t is the motor torque constant, and i_q is the (torque producing) q -axis component of the motor current, which is related to the phase currents of the PMSM by the Clarke–Park transformations. B_m^* is the coefficient for the effective viscous friction torque acting on the motor shaft representing a linear approximation to the true nonlinear friction characteristic. Repeating the process for the small workpiece required only one torsional mode, i.e., $J_3 = 0$ and $\theta_1 = \theta_3$.

Using standard system identification techniques, e.g., Ref. [13], the model for both workpieces can be parameterized from the input–output data as shown in Table 2.

2.3 Stability Analysis for System With Conventional Assumptions.

Using the parameters from Table 2 to construct the open-loop transfer function from motor current to motor velocity, reveals a large resonance at 443 Hz for the large workpiece configuration, which is similar to the frequency of the observed limit-cycle in Fig. 2, and gives some faith in the plant model.

However, when using the models to plot the closed-loop pole maps in Fig. 5, it is apparent that all the poles are within the unit circle, suggesting that both axis configurations are stable. This result is not consistent with the experimentally observed instability (limit-cycle) that occurs when the large workpiece is loaded into the machine. Consequently, the assumptions made in deriving the system model will be revisited in Sec. 3 through the inclusion of computation delays and the fast-rate current loop/electrical system on the overall dynamics of the system, and an investigation of the linear friction assumption in Eq. (1).

3 Removal of Simplifying Assumptions

The simplifying assumptions on the controller and plant dynamics used in obtaining the models in Sec. 2 will now be removed in order to test which aspects are crucial to reproducing the observed limit-cycle phenomenon.

3.1 Inclusion of Fast Controller Dynamics. The fast controller dynamics that will now be considered consist of a computation delay in the industrial controller, the current controller along with current reference filters, and the electrical system dynamics. The code executing on an industrial DSP has a known delay of $2T$ in calculating the output of the velocity controller. This may be represented at the fast sample-rate $1/T$ as

$$C_D(z) = \frac{1}{z^2} \quad (2)$$

Similarly, it is known that a first-order filter is implemented on the DSP at the fast sample-rate with transfer function

$$C_{LP}(z) = \frac{0.0991(z + 1)}{z - 0.8019} \quad (3)$$

Finally, the current controller (which includes Clarke–Park transforms) and electrical system must be identified from the input–output data. The result of this system identification leads to a fast sample-rate model of the form

$$C_{ES}(z) = \frac{0.05573(z + 0.9748)}{z^2 - 1.827z + 0.9264} \quad (4)$$

Equations (2)–(4) can be combined into a single discrete-time state space representation. To combine the fast sample-rate system with the previously specified plant dynamics and position/velocity controller operating at the slower rate ($\frac{1}{pT}$), a multirate system analysis technique known as *lifting in the time domain* is used [14,15]. An example of this approach applied to a multirate cascaded proportional integral derivative (PID) controller is presented in Ref. [16].

Using the default controller parameters from Table 1 to plot the closed-loop poles of the position loop, Figs. 6(a) and 6(b), reveals that the system is stable for the small workpiece configuration, but unstable when replaced with the large workpiece. Note that, for this result to be obtained, the dynamics from *all* the fast sample-rate elements considered here must be included. The frequency of the unstable poles shown in Fig. 6(b) is found to be approximately 445 Hz, which agrees well with the experimentally observed oscillations of Fig. 2.

A classical solution used in the industry for dealing with the instability is to notch filter the current reference at the resonant frequency [8] in order to attenuate control inputs that lead to excitation of the vibrational mode. This can be achieved by augmenting the low-pass filter model with a notch filter with transfer function

$$C_N(z) = \frac{0.9352(z^2 - 1.9774z + 1)}{z^2 - 1.8492z + 0.8651} \quad (5)$$

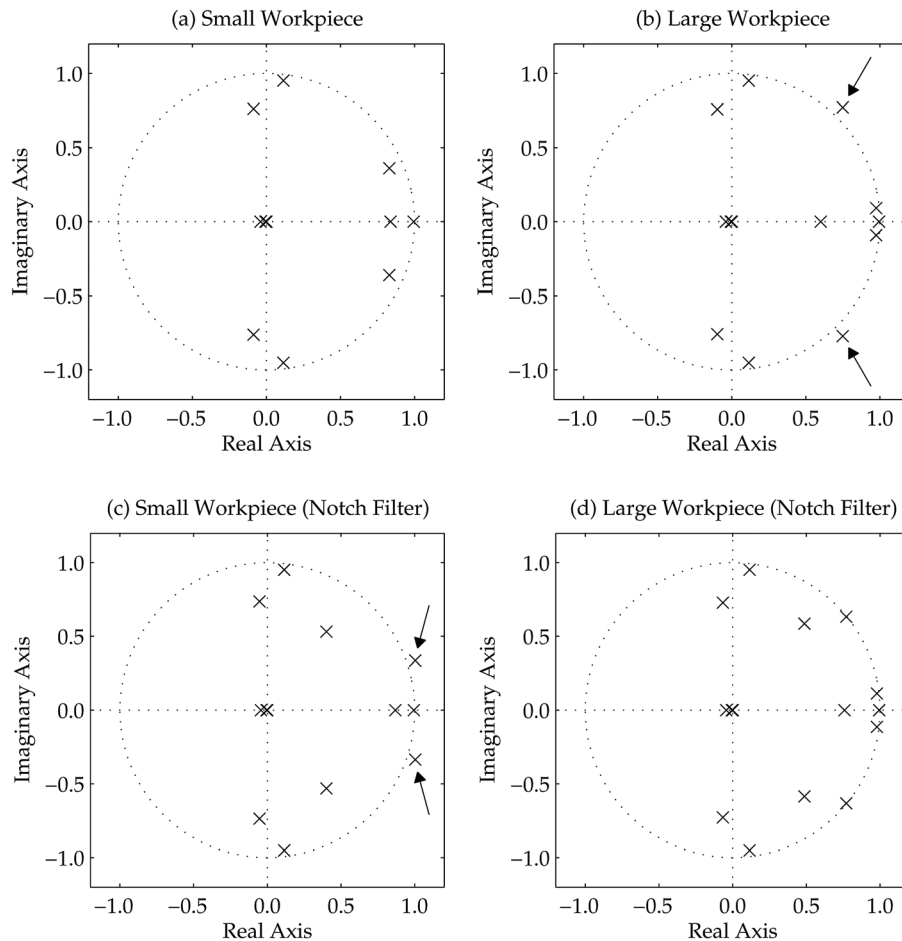


Fig. 6 Closed-loop poles of the motor position loop for the discrete model of the servo drive axis loaded with both small and large workpieces—the model includes the fast sample-rate elements for (a) and (b), and additionally, a notch filter for (c) and (d)

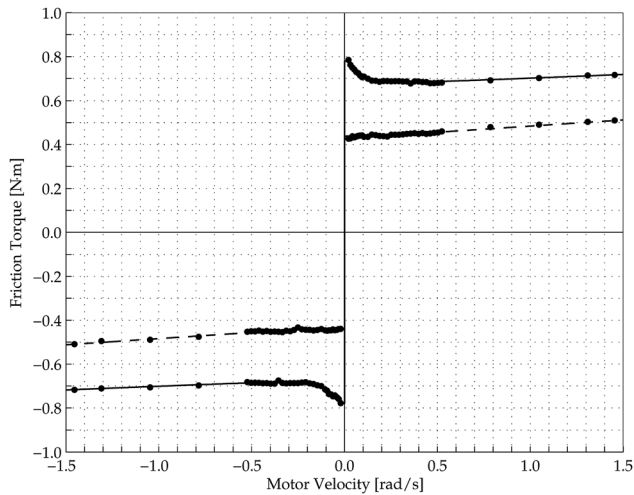


Fig. 7 Friction model experimental data (dots) and model fit for both small (dashed line) and large (solid line) workpieces

This addition results in the closed-loop poles shown in Figs. 6(c) and 6(d). Note that for the large workpiece the system is now stable, but for the small workpiece the addition of the notch filter actually destabilizes the system. Again, both of these outcomes agree with experimentally observed phenomena.

Consequently, for this case study, it is apparent that the fast sample-rate elements *must* be considered for the analytic study to

Table 3 Friction model parameters

Parameter	Small workpiece	Large workpiece	Unit
T_c	0.4271	0.6661	N m
B_m	0.0567	0.0346	N m/(rad/s)
T_{st}	0.0109	0.1144	N m
ω_s	0.1393	0.0770	rad/s

agree with the experimental observations. However, there is a caveat on this conclusion. Since linear analysis techniques have been used, the friction model also had to be linear. Given the actual friction is known to be nonlinear about zero velocity, it is prudent to investigate what effect, if any, this has on the results presented.

3.2 Inclusion of Dynamic Friction Effects. In Sec. 3.1, the friction acting on the motor shaft was assumed to be purely viscous (i.e., linear), which allowed classical linear system analysis tools to be used. In reality, the friction is strongly nonlinear about zero velocity as indicated in Fig. 7, which was obtained from a series of constant velocity experiments for each workpiece and agrees with the nonlinear steady-state model presented in Ref. [9]

$$T_f(\omega_m) = \left(T_c + B_m |\omega_m| + \frac{T_{st}}{1 + (\omega_m/\omega_s)^2} \right) \text{sgn}(\omega_m) \quad (6)$$

Here, ω_m is the motor shaft (J_1) velocity, T_c is the Coulomb friction, B_m is the viscous damping coefficient, T_{st} is the

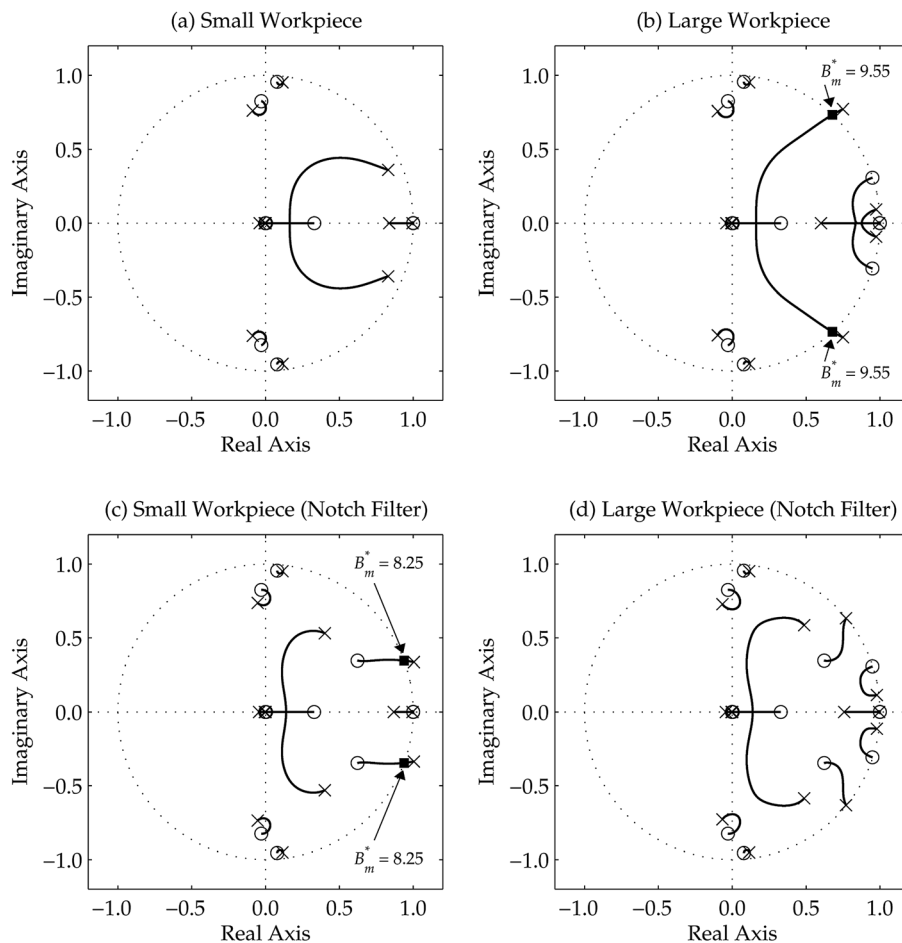


Fig. 8 Root locus for closed position loop with default tuning for (a) and (b), and with default tuning and a notch filter for (c) and (d), for both small and large workpieces in each case. The loci show the effect of varying the effective viscous friction coefficient.

magnitude of the Stribeck friction, and ω_s is the characteristic velocity of the Stribeck friction. The total friction torque at breakaway, known as the static friction torque, is $T_s = T_c + T_{st}$. The experimentally identified model parameters are shown in Table 3.

This nonlinear friction acts like a large effective viscous friction, B_m^* in Eq. (1) at small shaft velocities, and B_m^* decreases as the velocity increases. To capture the dependence of the effective viscous friction coefficient on periodic shaft velocity perturbations in a way that is readily incorporated into the linear model, a describing function-like analysis technique is proposed [17], whereby the energy dissipated over one period of the velocity perturbation $\omega_m = A \sin(\omega t)$ for the nonlinear friction model (6) and the linear friction model, $T_f^* = B_m^* \omega_m$, are equated to give

$$B_m^* = \frac{\int T_f \omega_m dt}{\int \omega_m^2 dt} = \frac{4T_c}{A\pi} + B_m + \frac{2\omega_s^2 T_{st}}{A^2 \pi \sqrt{\omega_s^2 + A^2}} \ln \left(\frac{\sqrt{\omega_s^2 + A^2} + A}{\sqrt{\omega_s^2 + A^2} - A} \right) \quad (7)$$

From Eq. (7), it is apparent that the effective viscous friction coefficient, B_m^* , decreases monotonically with A . In the system identification of Sec. 2.2, the value obtained for the effective viscous friction was $B_m^* = 0.0264 \text{ N m/(rad/s)}$. To confirm that the stability analysis is valid with this value, it is necessary to investigate the effect the viscous damping coefficient has on the linear system stability.

Figures 8(a) and 8(b) show the position-loop root locus for the axis with both small and large workpieces for the default controller tuning, where the parameter varying is B_m^* . For the large workpiece, the squares show the point at which the unstable closed-loop poles transition into the stable region. This occurs at $B_m^* = 9.55 \text{ N m/(rad/s)}$. Substituting $B_m^* = 9.55 \text{ N m/(rad/s)}$ into Eq. (7) leads to a critical sinusoidal velocity amplitude of 0.097 rad/s .

Figures 8(c) and 8(d) show the root locus for the axis with both small and large workpieces for the default controller tuning, plus the notch filter located to attenuate control inputs that lead to excitation of the first vibrational mode of the large workpiece configuration. For the small workpiece, the squares show the point at which the unstable closed-loop poles transition into the stable region. This occurs at $B_m^* = 8.25 \text{ N m/(rad/s)}$, and corresponds to a critical sinusoidal velocity amplitude of 0.068 rad/s .

Thus, provided the initial perturbation invokes a velocity of greater than 0.097 rad/s the axis will transition into the unstable operating region, the magnitude of the oscillations will increase, thus decreasing the effective viscous friction and further destabilizing the system.

4 Conclusions and Future Work

This paper has demonstrated that in order to successfully design model-based controllers for direct-drive machine tool axes with lightly damped structural vibrations, it may not be sufficient to simply model the mechanical dynamics and neglect those of the electrical system. In fact, in the case investigated in this paper, accurate modeling of the current servo (taking account of multirate sampling and computation delays) was more significant in predicting experimentally observed limit-cycles than was increasing the number of vibrational modes in the mechanical plant model.

To validate the decision to use linear friction models in the stability analysis, the effect of nonlinear friction on the overall dynamics of the system was investigated. The analysis showed that given certain conditions, in this case a sufficiently large disturbance, the effective viscous friction is reduced to the point where linear analysis will correctly predict instability in the system.

Finally, it was demonstrated that given the high level of tuning necessary to meet the performance requirements, a cascaded PID controller with fixed gains and filters is not ideally suited for controlling a direct-drive axis, which is subject to large changes in load dynamics. Future work in this area will concentrate on using the low-order linear models developed in this paper to produce an adaptive control approach that results in optimal performance over a large range of possible axis configurations and the ensuing dynamics. Future research may also consider the possibility of normalizing the system parameters through appropriate scaling, and thus identify a link between the mechanical resonance and the phase lag introduced by the combination of multirate servo loops and computation delays which results in closed-loop instability.

References

- [1] del Re, L., Kaiser, O., and Pfiffner, R., 1996, "Black Box Identification and Predictive Control of High Speed Machine Tools," *Proceedings of the IEEE International Conference on Control Applications*, pp. 480–485.
- [2] Erkorkmaz, K., and Altintas, Y., 2001, "High Speed CNC System Design. Part II: Modeling and Identification of Feed Drives," *Int. J. Mach. Tools Manuf.*, **41**(10), pp. 1487–1509.
- [3] Zheng, J., Zhang, M., and Meng, Q., 2006, "Modeling and Design of Servo System of CNC Machine Tools," *Proceedings of the IEEE International Conference on Mechatronics and Automation*, pp. 1964–1969.
- [4] Younkin, G. W., McGlasson, W. D., and Lorenz, R. D., 1991, "Considerations for Low-Inertia AC Drives in Machine Tool Axis Servo Applications," *IEEE Trans. Ind. Appl.*, **27**(2), pp. 262–267.
- [5] Poinet, P., Gautier, M., and Khalil, W., 1999, "Modeling, Control and Simulation of High Speed Machine Tool Axes," *Proceedings of the IEEE/ASME International Conference on Advanced Intelligent Mechatronics*, pp. 617–622.
- [6] Moscrop, J., Cook, C., and Moll, P., 2001, "Control of Servo Systems in the Presence of Motor-Load Inertia Mismatch," *Proceedings of the IEEE Industrial Electronics Society Conference*, Vol. 1, pp. 351–356.
- [7] Gannel, L., and Welch, R. H., Jr., 2003, "Improving the Dynamic Motion Behavior of a Servo System With Low Mechanical Stiffness," *Proceedings of the IEEE Industry Applications Society Annual Meeting*, Vol. 1, pp. 40–44.
- [8] Ellis, G., and Lorenz, R. D., 2000, "Resonant Load Control Methods for Industrial Servo Drives," *Proceedings of the IEEE Industry Applications Society Annual Meeting*, Vol. 3, pp. 1438–1445.
- [9] Armstrong-Hélouvry, B., Dupont, P., and de Wit, C. C., 1994, "A Survey of Models, Analysis Tools and Compensation Methods for the Control of Machines With Friction," *Automatica*, **30**(7), pp. 1083–1138.
- [10] Kelly, M. J., and Toncich, D. J., 2000, "Overcoming Encoder Quantisation Noise in an Adaptive Position Controller," *Int. J. Mach. Tools Manuf.*, **40**(14), pp. 2031–2046.
- [11] Krishnan, R., 2001, *Electric Motor Drives: Modeling, Analysis, and Control*, Prentice-Hall, Upper Saddle River, NJ.
- [12] Ebrahimi, M., and Whalley, R., 2000, "Analysis, Modeling and Simulation of Stiffness in Machine Tool Drives," *Comput. Ind. Eng.*, **38**(1), pp. 93–105.
- [13] Ljung, L., 1999, *System Identification: Theory for the User*, 2nd ed., Prentice-Hall, Upper Saddle River, NJ.
- [14] Berg, M. C., Amit, N., and Powell, J. D., 1988, "Multirate Digital Control System Design," *IEEE Trans. Autom. Control*, **33**(12), pp. 1139–1150.
- [15] Tomizuka, M., 2004, "Multi-Rate Control for Motion Control Applications," *Proceedings of the IEEE International Workshop on Advanced Motion Control*, pp. 21–29.
- [16] Stephens, M. A., Manzie, C., and Good, M. C., 2010, "On the Stability Analysis and Modelling of a Multirate Control Direct-Drive Machine Tool Axis Subject to Large Changes in Load Dynamics," *Proceedings of the American Control Conference*, pp. 1550–1555.
- [17] Thomson, W. T., and Dahleh, M. D., 1998, *Theory of Vibration With Applications*, 5th ed., Prentice-Hall, Upper Saddle River, NJ.